PCCP

Accepted Manuscript

This is an *Accepted Manuscript*, which has been through the Royal Society of Chemistry peer review process and has been accepted for publication.

Accepted Manuscripts are published online shortly after acceptance, before technical editing, formatting and proof reading. Using this free service, authors can make their results available to the community, in citable form, before we publish the edited article. We will replace this *Accepted Manuscript* with the edited and formatted *Advance Article* as soon as it is available.

You can find more information about *Accepted Manuscripts* in the Information for Authors.

Please note that technical editing may introduce minor changes to the text and/or graphics, which may alter content. The journal's standard Terms & Conditions and the Ethical guidelines still apply. In no event shall the Royal Society of Chemistry be held responsible for any errors or omissions in this *Accepted Manuscript* or any consequences arising from the use of any information it contains.

ROYAL SOCIETY OF CHEMISTRY

www.rsc.org/pccp

Facile preparation and enhanced microwave absorption properties of core-shell composite spheres composited of Ni cores and TiO_2 shells

Biao Zhao [a], Gang Shao [a] *, Bingbing Fan [a], Wanyu Zhao [a], Yajun Xie [a], Rui Zhang [a, b] *

Received (in XXX, XXX) Xth XXXXXXXXX 20XX, Accepted Xth XXXXXXXXX 20XX
DOI: 10.1039/c000000x

ABSTRACT: Core-shell microspheres with Ni cores and two phases of TiO_2 (anatase, rutile) shells have been successfully synthesized. The crystal structure, morphology and microwave absorption properties of the as-prepared composites were analyzed by X-ray diffraction, field-emission scanning electron microscopy, energy dispersive X-ray spectroscopy, transmission electron microscopy, and vector network analysis. The core-shell rutile TiO_2-coated Ni exhibits better antioxidation ability than that of pure Ni due to the presence of rutile TiO_2 shell, which is confirmed by the thermalgravimetric analysis (TGA). In comparison with bared Ni, these two composites show better microwave absorption properties. The minimum reflection loss (RL) is –38.0 dB at 11.1 GHz with only thickness of 1.8 mm for the Ni@TiO_2 (rutile) composite. The enhanced absorption capability arises from the efficient complementarities between the magnetic loss and dielectric loss, multiple interfacial polarization, high thermal conductivity of rutile TiO_2 and microwave attenuation constant. These results show that rutile TiO_2-coated Ni composite is a great potential microwave absorbing material with thin thickness and high-efficiency of practical applications.

1. Introduction

With the explosive development of communication technology and high-frequency circuit devices operated in the gigahertz (GHz) range, electromagnetic interference (EMI) has become a great issue. EMI pollution plays a negative effect in the systems applied for commercial, medical and industrial applications. Microwave absorbing materials which can deal with the serious EM interference issues have been intrigued intense attention.[1-4] These materials can dissipate or absorb microwaves effectively, which converts energy into heat or other styles. [5-15]

In recent years, core–shell structures, have been focused on because of their enhanced microwave absorption property through cooperation between the components, such as Fe_3O_4-poly(3,4-ethylenedioxythiophene) microspheres, [16] porous Fe_3O_4/carbon nanorods, [17] ZnO-coated iron, [18] Ni/ZnS, [19] Ni/SnO_2 microspheres, [20] Fe_3O_4/ZnO nanorods, [21] SiO_2@$FeNi_3$, [22] Fe_3O_4/SnO_2 nanorods, [23] Ni/polyaniline, [24] carbon-coated nickel. [25] Generally, among these materials, the magnetic materials acted as cores, which enhance the permeability of the composites, resulting in increasing the magnetic loss. The dielectric materials as shells, which regards as an electric polarization centre and insulating matrix, give rise to the improved dielectric loss and good impedance match. The excellent microwave absorption ability can be attained due to enhanced magnetic loss, dielectric loss, good impedance match and suppression of eddy current loss. [26] Therefore, dielectric–magnetic composites are beneficial for achieving excellent microwave absorption properties. Recently, the microwave absorption properties of metal Ni particles have been attracted intense attention [27-29] owing to its large saturation magnetization and high Snoek's limit at high frequency bands. [22] However, the high conductivity results in the rapid decrease in high frequency permeability due to eddy current losses induced by electromagnetic wave. [30] An effective strategy to solve this problem is to cover the Ni metallic particles by an inorganic or nonmagnetic coating to create core/shell structures. [31]

TiO_2 (Titanium oxide) is an important semiconductor which possesses thermally stable properties and high relative dielectric constant, so it can be used for potential application in microwave absorption. [32-34] Liu and co-workers have synthesized composite microspheres with Fe_3O_4 cores and hierarchical TiO_2 shells and the Fe_3O_4@TiO_2 core–shell microspheres exhibit the lower reflection loss and wider absorption frequency range than pure Fe_3O_4. [35] Chen and co-workers have successfully prepared Fe_3O_4/TiO_2 core/shell nanotubes with outstanding microwave absorption properties. [36] The composite composed of Fe_3O_4 and

Physical Chemistry Chemical Physics Accepted Manuscript

TiO_2 possesses both the advantages of unique magnetic properties of Fe_3O_4 and strong dielectric characteristics of TiO_2, which offer the excellent microwave absorption abilities of this kind of materials.

To the best of our knowledge, there are scarce reports on the fabrication and microwave absorption properties of Ni-TiO_2 core/shell structures with Ni cores and TiO_2 (anatase and rutile) as shells. Herein, a facile and efficient method was introduced to synthesize core-shell Ni/TiO_2 composite microspheres with fcc Ni cores and anatase or rutile TiO_2 shells. The influences of preparation recipes on the crystal structure and morphology of Ni/TiO_2 (anatase) microspheres were investigated. Moreover, the microwave absorption abilities of these two composites have been studied based on complex permittivity and permeability. It can be found that the core-shell structured Ni/TiO_2 (rutile) microspheres show outstanding microwave absorption properties.

2. Experimental section

2.1. Materials. All chemicals were of analytical grade and used without further purification. Trisodium citrate, anhydrous ethanol, tetrabutyl orthotitanate (TBOT) and $N_2H_4{\cdot}H_2O$ (80%) were purchased from Guangfu Chemical Co. Ltd. (Tianjin, China). Nickel chloride hexahydrate ($NiCl_2{\cdot}6H_2O$), 1,2-isopropanol, $NH_3{\cdot}H_2O$ and sodium acetate were provided by Xilong Chemical Reagent Co. Ltd. (Guangdong, China). Ni/TiO_2 core-shell microspheres were fabricated through a two-step method.

2.2. Preparation of Ni microspheres. The Ni microspheres were prepared through a solvothermal reaction at 140 ºC by the reduction of $NiCl_2$ with hydrazine hydrate using sodium acetate as an alkali source, trisodium citrate as a stabilizer. Typically, $NiCl_2{\cdot}6H_2O$ (1.12 g, 5 mmol), sodium acetate (3.0 g) and trisodium citrate (0.3 g) were first dissolved in 1,2-propanediol (60 mL). Then 6 mL hydrazine hydrate was added under stirring. After that, the mixture was stirred vigorously for 20 min and then transferred into a Teflon-lined stainless steel autoclave. The autoclave was heated at 140 ºC and maintained for 15 h, and then allowed to cool to room temperature. Finally, the black precipitates were washed with distilled water and absolute ethanol and dried at 60 ºC for 12 h under vacuum.

2.3 Synthesis of Ni/TiO_2 core–shell microspheres

Preparation of Ni@TiO_2 (anatase) composites: The core/shell Ni/TiO_2 microspheres were synthesized via a templating approach. [37] The as-prepared Ni microspheres (0.05 g) were dispersed in 1,2-propanediol (50 mL), followed by the addition of $NH_3{\cdot}H_2O$ (6 mL). After stirring gently for 20 min, tetrabutyl orthotitanate (TBOT, 2 mL) was added to the solution. The mixture was then transferred into a Teflon-lined stainless steel autoclave and kept at 200 °C for 15 h. After that, the products were washed with distilled water and ethanol, and dried at 60 °C in vacuum overnight. The as-obtained Ni/TiO_2 (anatase) was denoted as Ni-A for the convenience of discussion. The effects of preparation recipes (temperature, the amounts of $NH_3{\cdot}H_2O$) on the phase and morphology of products were also investigated.

Preparation of Ni-TiO_2 (rutile) core-shell composite: The as-received Ni-A microspheres were annealing at 1000 °C under Ar gas protection for 2 h to get Ni@TiO_2 (rutile) composite particles. The Ni@TiO_2 (rutile) composite particles were denoted as Ni-R in following discussion.

2.4. Characterization. The crystal structure of the samples were characterized by X-ray diffraction (XRD, XD-3, Beijing Purkinje General Instrument Co. Ltd. Cu Kα radiation source, λ=0.15406 nm). The morphology, size and chemical composition of the synthesized samples were determined by field-emission scanning electron microscopy equipped with energy dispersive X-ray spectroscopy (FESEM/EDS; JSM-7001F) and transmission electron microscope (TEM, JEM-2100). The thermogravimetric analyzer (TGA) was performed on a STA 409/PC simultaneous thermal analyzer (Netzsch, Germany) from 50 ºC to 800 ºC in flowing air. The paraffin-composites were prepared by mixing the Ni/TiO_2 core/shell microspheres with 30 wt % wax, which are used for microwave measurement. The mixtures were then pressed into ring shaped samples (Φ_{out}: 7.00 mm, Φ_{inner}: 3.04 mm). The complex permittivity and permeability of the

Physical Chemistry Chemical Physics Accepted Manuscript

This journal is © The Royal Society of Chemistry [year]

composites were measured between 2.0-18.0 GHz through a vector network analyzer (Agilent N5244A).

3. Results and discussion

3.1 Synthesis and characterization of core-shell Ni/TiO_2 microspheres

Scheme 1 illustrates the preparation process of the core-shell Ni/TiO_2 composite microspheres. Firstly, uniform Ni microspheres were synthesized by a solvothermal reaction at 140 °C by reduction of $NiCl_2$ with hydrazine hydrate. Secondly, Ni-A composites were prepared through a template method using the as-prepared Ni microspheres as starting templates and TBOT as a precursor. Finally, the Ni-R composites were obtained after calcination of Ni-A at 1000 °C under Ar gas protection for 2 h.

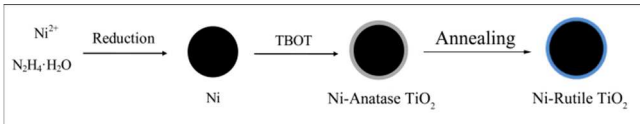

Scheme 1. Schematic illustration of the formation process of the core-shell Ni-A and Ni-R composite microspheres.

The phase identification and phase purity of the as-obtained products were characterized by XRD. **Fig. 1a** exhibits the XRD pattern of Ni particles. All the diffraction peaks can be well assigned to fcc phase of Ni (JCPDS card no. 04-0850). After coating with the TiO_2 layer, besides the diffraction peaks of Ni, new characteristic diffraction peaks (**Fig. 1b**) are obviously observed, which can be assigned to anatase TiO_2 (JCPDS card no. 21-1272). It suggests that the composites were composed of Ni and anatase TiO_2. **Fig. 1c** shows the XRD pattern of the products obtained from the calcination of Ni-A. It can be found that the diffraction peaks can be assigned to the nickel and rutile TiO_2 (JCPDS card no. 21-1276). The diffraction peaks of anatase TiO_2 disappear, which indicates that the anatase TiO_2 phases have been completely transformed into rutile TiO_2 after high temperature annealing.

Fig. 2a shows the typical FESEM image of the Ni particles, which possess uniform spherical shape and the diameter of 0.7−1.0 μm. The citrate groups could ground on the particle surface during the solvothermal reaction and thus facilitate the subsequent coating with the TiO_2 layer. [38] **Fig. 2b,c** show the FESEM images of the obtained Ni-A microspheres with the diameter of 0.8−1.1 μm. One significant difference is clearly observed between Ni-A microspheres and naked Ni microspheres. The difference is that the surfaces of Ni-A microspheres are rougher than those of bared Ni microspheres, which indicates Ni microspheres were coated by TiO_2 layer to form core-shell structure. **Fig. 2d** presents the morphology of Ni-R products. It is noteworthy that the uniform Ni microspheres were densely coated by lots of rutile TiO_2 particles. Compared with anatase TiO_2, the sizes of TiO_2 become bigger due to annealing process.

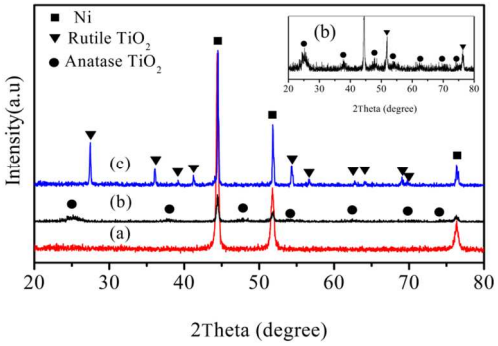

Fig. 1 XRD patterns of (a) Ni microspheres, (b) Ni-A microspheres and (c) Ni-R composite microspheres; inset shows the enlarged XRD curve of Ni-A microspheres.

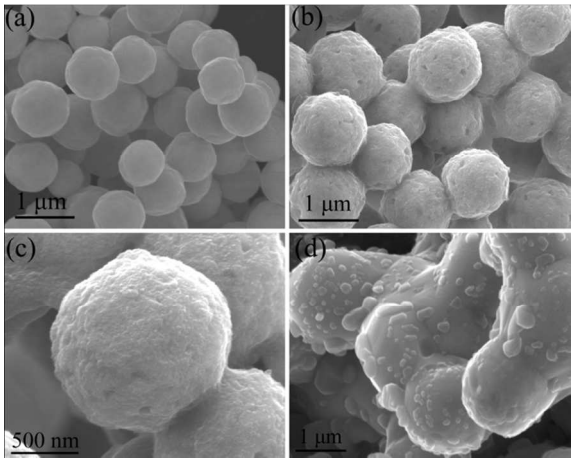

Fig.2 (a) FESEM images of Ni microspheres, (b,c) different magnification FESEM images of Ni-A composite and (d) FESEM image of Ni-R composite

Physical Chemistry Chemical Physics Accepted Manuscript

To discerned the thickness of the TiO_2 shells and get more information of Ni/TiO_2 composites, the TEM images of Ni-A and Ni-R composites were examined, as shown in Fig. 3(a,c). The thicknesses of anatase TiO_2 and rutile TiO_2 shells are about 20-50 nm and 20-60 nm, respectively. Moreover, the sizes of Ni cores kept constant (~1 μm) after annealing process. The insets of Fig.3 (a,c) exhibit the HRTEM images of anatase TiO_2 and rutile TiO_2, respectively. The lattice spaces of 0.35 nm and 0.32 nm are in good agreement with (101) plane of anatase TiO_2 and (110) plane of rutile TiO_2, respectively. Additionally, the selected area electron diffraction (SAED) rings confirmed the identity of the anatase TiO_2 (Fig.3b) and rutile TiO_2 (Fig.3d), and the characteristic spaces were indicative of the anatase TiO_2 and rutile TiO_2 on the surfaces of Ni particles , in good agreement of the XRD and HRTEM results in Fig. 1 and Fig. 3 (a,c).

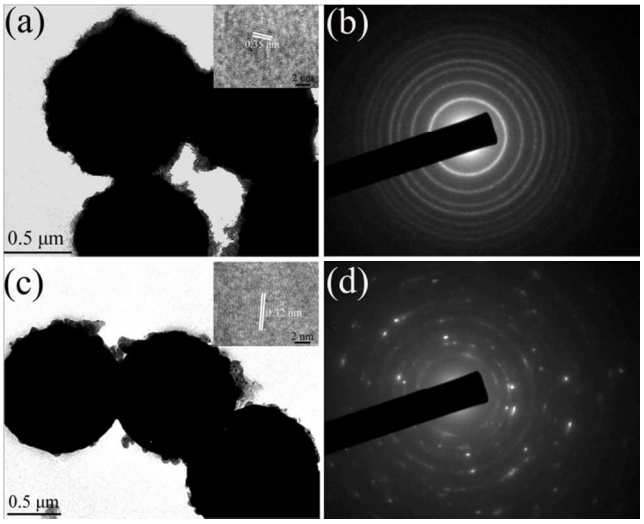

Fig.3 (a) TEM image and (b) SAED pattern of Ni-A composite, and the inset (a) shows the HRTEM image of Ni-A sample; (c) TEM image and (d) SAED pattern of Ni-R composite, and the inset (c) shows the HRTEM image of Ni-R composite.

The EDS pattern of the Ni-A, shown in **Fig. 4b**, indicates that the obtained heterostructures are composed of Ni, Ti and O elements. The C element signal originates from the carbon conductive tape to support samples during the test. One composite microsphere (Ni-A) was choose to further investigate Ni-A microstructure (**Fig. 4a**), the elemental mappings of Ni/TiO_2 were performed in **Fig. 4c-e**. The Ni element can be clearly detected in the core region, while the O element and Ti element can be detected in the shell regions, which further confirms the unique core-shell structures with Ni cores and TiO_2 shells.

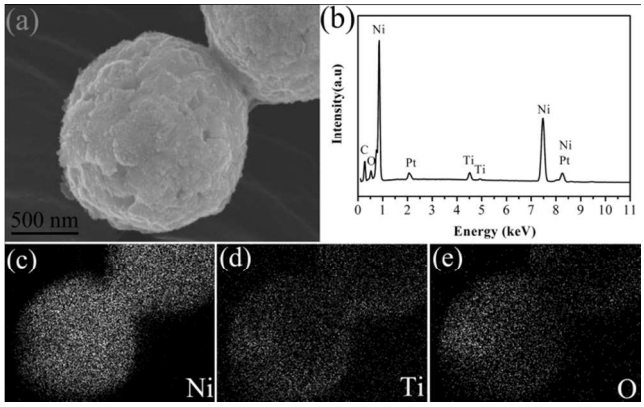

Fig. 4 (a) FESEM image of the Ni@TiO_2 core−shell microsphere, (b) EDS pattern of Ni-A composite microspheres and (c-e) elemental mappings of Ni, Ti and O.

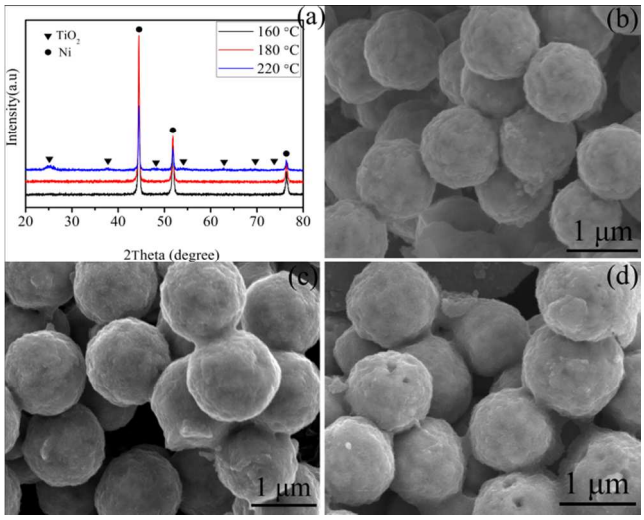

Fig. 5 (a) XRD patterns and (b-d) SEM images of the Ni/TiO_2 products formed after 15 h at various temperatures: (b) 160, (c) 180, and (d) 220 ºC.

The influences of temperature on the phase and morphology of such core-shell Ni-A microspheres were investigated. It can be clearly seen in **Fig. 5b-d** that the original Ni microspheres are coated with TiO_2 shells at different temperatures. However, as shown in **Fig. 5a**, the phases of TiO_2 shells prepared at low temperature (160 ºC, 180 ºC) are amorphous. When the temperature increases to 200 ºC, the anatase TiO_2 appear (**Fig.**

Physical Chemistry Chemical Physics Accepted Manuscript

This journal is © The Royal Society of Chemistry [year]

1b). When the temperature was further increased, the phase and shape of Ni/TiO_2 microspheres remain unchanged. This result suggests that a suitable temperature is necessary for the synthesis of the Ni/ anatase TiO_2 composite microspheres.

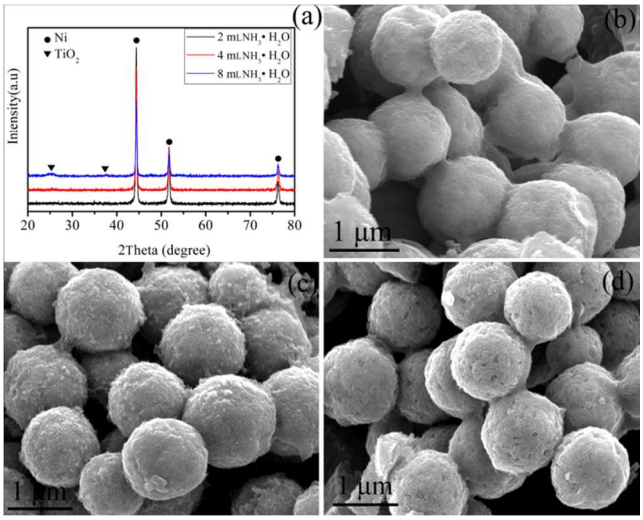

Fig. 6 (a) XRD patterns and (b-d) SEM images of as-prepared Ni/TiO_2 samples produced at various concentration of $NH_3{\cdot}H_2O$: (b) 2 mL, (c) 4 mL, and (d) 6 mL.

Notably, the concentration of $NH_3{\cdot}H_2O$ also plays a vital role in the final crystal structure of the Ni-A microspheres (**Fig. 6a**). The amorphous TiO_2 shells were obtained (< 6 mL $NH_3{\cdot}H_2O$). As the concentration of $NH_3{\cdot}H_2O$ increased to 6 mL $NH_3{\cdot}H_2O$, the Ni microspheres were successfully coated by anatase TiO_2 shells (**Fig.2b**). When the $NH_3{\cdot}H_2O$ contents further increased to 8 mL, the phase of TiO_2 shell was still anatase. From the **Fig. 6b-d**, it can be found that the core-shell structures with Ni cores and TiO_2 (amorphous or anatase) shells have been synthesized at different concentration of $NH_3{\cdot}H_2O$. It is comprehensive that we chose 6 mL $NH_3{\cdot}H_2O$ to synthesize such core-shell Ni/anatase TiO_2. The sol−gel process of a titanium alkoxide to form a polymerized TiO_2 networks is consisted of hydrolysis and condensation steps. The kinetics of hydrolysis and condensation over TBOT are mainly controlled by the concentration of ammonia while maintaining other reaction parameters constant.[39] At low concentration of ammonia, the hydrolysis and condensation rate of TBOT is very slow, resulting in a low concentration of titanium oligomers. Some amorphous TiO_2 nanoparticles are formed on the surface of Ni microspheres. When the amount of ammonia reach 6.0 mL, the hydrolysis and condensation of TBOT can be promoted, thus leading to a quick increasing of titanium oligomers. [40] A vital heterogeneous nucleation of TiO_2 occurs on the surface of Ni microspheres. Therefore, uniform TiO_2 shells are formed.

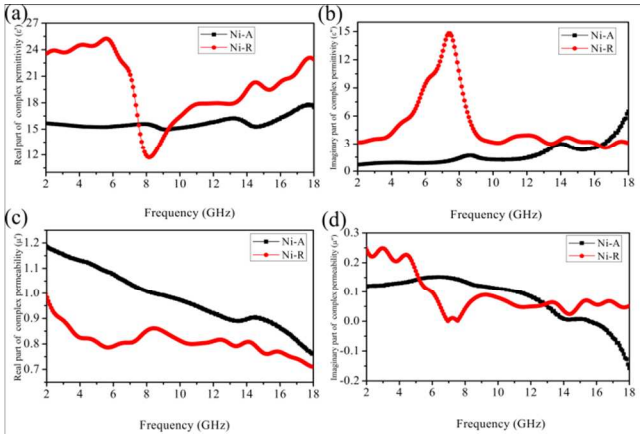

Fig. 7 Frequency dependence of (a) real part and (b) imaginary part of the relative complex permittivity, (c) real part and (d) imaginary part of the relative complex permeability for the Ni-A and Ni-R composites.

3.2 Electromagnetic parameters of Ni@TiO_2/paraffin composite

To investigate the microwave absorption properties of Ni/TiO_2 (Ni-A, Ni-R) samples, the electromagnetic parameters (relative complex permittivity, ε_r, and relative complex permeability, μ_r) of the paraffin-composites containing 70 wt % of the Ni/TiO_2 core/shell microspheres were measured at room temperature. **Fig. 7a** shows the frequency dependence of the real parts (ε') of relative complex permittivity ($\varepsilon_r = \varepsilon' - j\varepsilon''$) of the Ni-A and Ni-R wax-composites. The ε' values of Ni-R are mostly higher than that of Ni-A at frequency region over 2-18 GHz, which means higher polarization occurring in the Ni-R samples. The ε'' of Ni-R also shows higher values compared with Ni-A sample, which indicates larger dielectric loss **(Fig. 7b)**. It is intriguing that the ε' exhibits minimum value and ε'' shows maximum value at round 8.0 GHz, which is associated with resonant behavior. [41] The complex permeability of the core/shell Ni-A and Ni-R wax-composites (**Fig. 7c,d**) indicates that the μ'

Physical Chemistry Chemical Physics Accepted Manuscript

and μ″ decrease with increasing frequency. The μ′ values of the Ni-A and Ni-R samples decline from 1.18 to 0.76 and 0.99 to 0.71 over the 2–18 GHz, respectively. The μ″ values of Ni-A and Ni-R are in the range of -0.16 to 0.15 and 0.0005−0.25. It is found that the μ" of Ni-R microspheres are higher than that of Ni-A microspheres at frequency region about 2-5 GHz and 13-18 GHz. Based on the SEM (Fig. 2) and TEM (Fig.3), it can be found that the Ni particles are not completely coated by rutile TiO_2. The bared Ni cores can connect with each other to form current. As a result, the μ" of Ni-R shows higher than that of Ni-A microspheres at low frequency (2-5 GHz). At high frequency (f > 8.5 GHz), the eddy current loss of Ni-R leads to low value of μ″. In general, the microwave absorption is contributed by both dielectric loss and magnetic loss. However, for the Ni-A, the Ni cores were absolutely coated by anatase TiO_2 shells. At high frequency (f > 8.5 GHz), the dielectric loss (conductive loss) are main contribution to the microwave absorption. The magnetic loss is negligible. Thus, the μ" of Ni-A microspheres is lower than that of Ni-R microspheres. Interestingly, for the Ni-A, it is found that the μ″ value is negative between 15.62 and 18 GHz. Generally, for left-hand materials both permittivity and permeability are negative. However, only the μ″ value of the Ni/TiO_2 microspheres is negative. Therefore, the phenomenon should not be attributed to left-hand properties of the materials. Such phenomenon can be explained as the magnetic energy being radiated out form the composites. [23, 42, 43]

The electromagnetic absorption properties of absorbers are also dependent on the combination between magnetic loss and dielectric loss. [17, 44] The dielectric loss tangent ($\tan\delta_\varepsilon = \varepsilon''/\varepsilon'$) and magnetic loss tangents ($\tan\delta_\mu = \mu''/\mu'$) of Ni/TiO_2 samples are shown in **Fig. 8**. For the Ni-A, the $\tan\delta_\mu$ values are higher than 0.1 located at 2-11.6 GHz, which indicate that the magnetic loss plays a crucial role in the EM absorption at the low-frequency range. For the Ni-R, the $\tan\delta_\mu$ values are higher than 0.2 located at 2-4.8 GHz and $\tan\delta_\varepsilon$ are higher than $\tan\delta_\mu$ in the frequency of 4.8-18 GHz. In general, the EM wave absorptions are strongly dependent on the efficient complementarities between the magnetic loss and dielectric loss. Only dielectric loss or magnetic loss leads to poor EM attenuation. The Ni/TiO_2 core/shell microspheres prepared in the present work exhibit strong magnetic loss at low-frequency range and significant dielectric loss at high-frequency range. Such complementarities between the dielectric loss and magnetic loss indicate that the core/shell $Ni@TiO_2$ microspheres possess excellent EM absorption properties. It is worth noting that the whole tangent losses (magnetic loss and dielectric loss) of Ni-R are higher than those of Ni-A samples, which means the better microwave absorption properties of Ni-R sample.

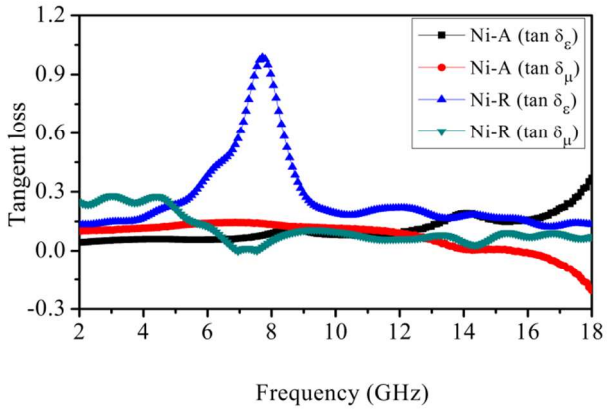

Fig. 8 The tangent loss of Ni-A and Ni-R core/shell microspheres.

Debye dipolar relaxation can be considered as an important mechanism to account for the dielectric loss of materials. The relative complex permittivity ε_r can be described as:[45, 46]

$$\varepsilon_r = \varepsilon_\infty + \frac{\varepsilon_s - \varepsilon_\infty}{1 + j2\pi f\tau} = \varepsilon' - j\varepsilon'' \qquad (1)$$

in which ε_s , ε_∞ , f , τ are the static permittivity, relative dielectric permittivity at the high-frequency limit, frequency and polarization relaxation time, respectively. Thus, ε′ and ε″ can be described by

$$\varepsilon' = \varepsilon_\infty + \frac{\varepsilon_s - \varepsilon_\infty}{1 + (2\pi f)^2\tau^2} \qquad (2)$$

$$\varepsilon'' = \frac{2\pi f\tau(\varepsilon_s - \varepsilon_\infty)}{1 + (2\pi f)^2\tau^2} \qquad (3)$$

According to eqn (2) and (3), the relationship between ε′ and ε″ can be deduced

Physical Chemistry Chemical Physics Accepted Manuscript

This journal is © The Royal Society of Chemistry [year]

$$(\varepsilon' - \frac{\varepsilon_s + \varepsilon_\infty}{2})^2 + (\varepsilon'')^2 = (\frac{\varepsilon_s - \varepsilon_\infty}{2})^2 \qquad (4)$$

Thus, the plot of ε′ versus ε″ would be a single semicircle, generally denoted as the Cole–Cole semicircle. [47] Each semicircle corresponds to one Debye relaxation process. **Fig. 9** shows the ε′-ε″ curves of Ni/TiO_2 paraffin-composite (70 wt% Ni/TiO_2). Three Cole–Cole semicircles were found in Ni-A paraffin-composite and five semicircles in Ni-R wax-composites, indicating the existence of Debye relaxation process. The three relaxation processes of Ni-A sample may arise as follow: under the alternating electromagnetic field, the lag of induced charges from the TiO_2-TiO_2, TiO_2-paraffin, and Ni-TiO_2 interfaces which encounters the external applied field results in the relaxation and transfer the electromagnetic energy to thermal energy. Therefore, the microwave is attenuated. [48] And for Ni-R paraffin composite, besides the above mentioned TiO_2-TiO_2, TiO_2-paraffin, and Ni-TiO_2 interfaces, the various sizes of rutile TiO_2 can lead to multi-relaxation processes. The Debye relaxation of Ni@TiO_2 core-shell particles can be used to explain the dielectric loss, which is familiar with previous literature. [49] However, the Cole–Cole semicircles are distorted, indicating that except for the Debye relaxation, other mechanisms, such as Maxwell–Wagner relaxation and electron polarization, could be also existing in core-shell Ni/TiO_2 wax-composites. In core-shell structured composites, the additional interfaces can induce interfacial polarization (Maxwell–Wagner effect). [50] In addition, Ni and TiO_2 particles and different sizes of rutile TiO_2-TiO_2 particles, are responsible for interfacial polarization which further contribute to dielectric loss. Interfacial polarization occurs in heterogeneous media due to accumulation of charges at the interfaces.

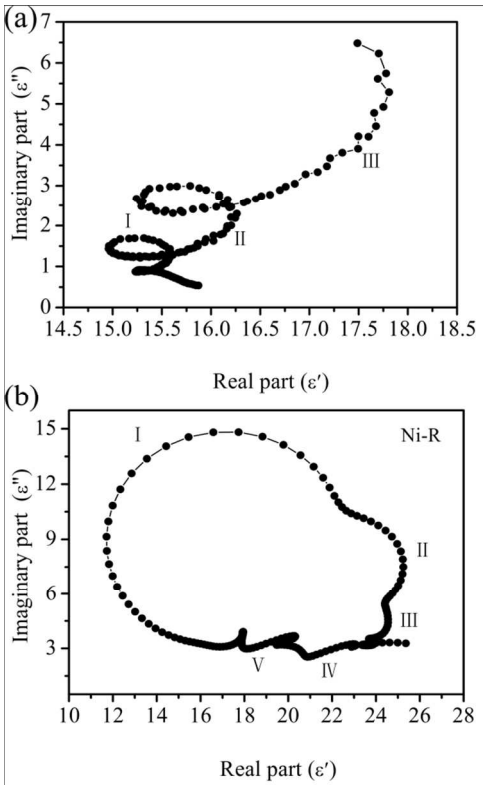

Fig. 9 The relation between real part (ε′) and imaginary part (ε″) of the complex permittivity (Cole–Cole plot) of (a) Ni-A and (b) Ni-R composites.

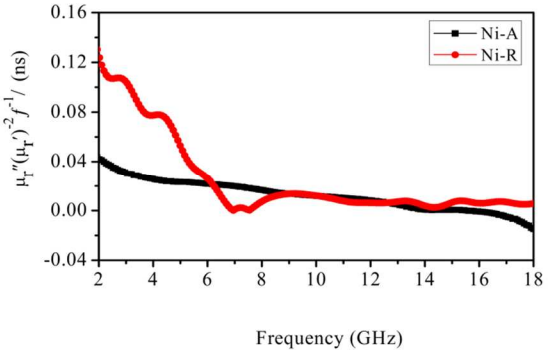

Fig. 10 The value C_0 of $\mu''(\mu')^{-2} f^{-1}$ as a function of frequency of (a) Ni-A and (b) Ni-R composites.

Generally, in the microwave frequency band, magnetic loss mainly comes from eddy current effects, natural resonance and exchange resonance. The eddy current loss is related to the diameter of particles (d) and the electric conductivity (σ), which can be expressed by [51] $\mu'' \approx 2\pi\mu_\circ(\mu')^2\sigma d^2 f/3$, where f is the applied frequency, μ_0 is the vacuum permeability. According to this equation, if the magnetic loss only originates from the eddy

Physical Chemistry Chemical Physics Accepted Manuscript

current loss, the values of $\mu''(\mu')^{-2}f^{-1} = 2\pi\mu_0\sigma d^2/3$ should be constant varying frequency. As shown in **Fig. 10**, in the Ni-A composite, the values of $\mu''(\mu')^{-2}f^{-1} = 2\pi\mu_0\sigma d^2/3$ decrease gradually with increasing frequency in the whole range of 2.0–18.0 GHz. Therefore, the magnetic loss in the present samples is caused mainly by the nature resonance and exchange resonance. However, the values of $\mu''(\mu')^{-2}f^{-1} = 2\pi\mu_0\sigma d^2/3$ remain approximately constant when f > 8.5 GHz for the Ni-R sample, which confirms that magnetic loss is caused mainly by the eddy current loss in this frequency band. The natural resonance occurs usually at low frequency and the exchange resonances at high frequency. The multi-peaks in the μ″ can be attributed to the natural resonance and exchange resonance.[52]

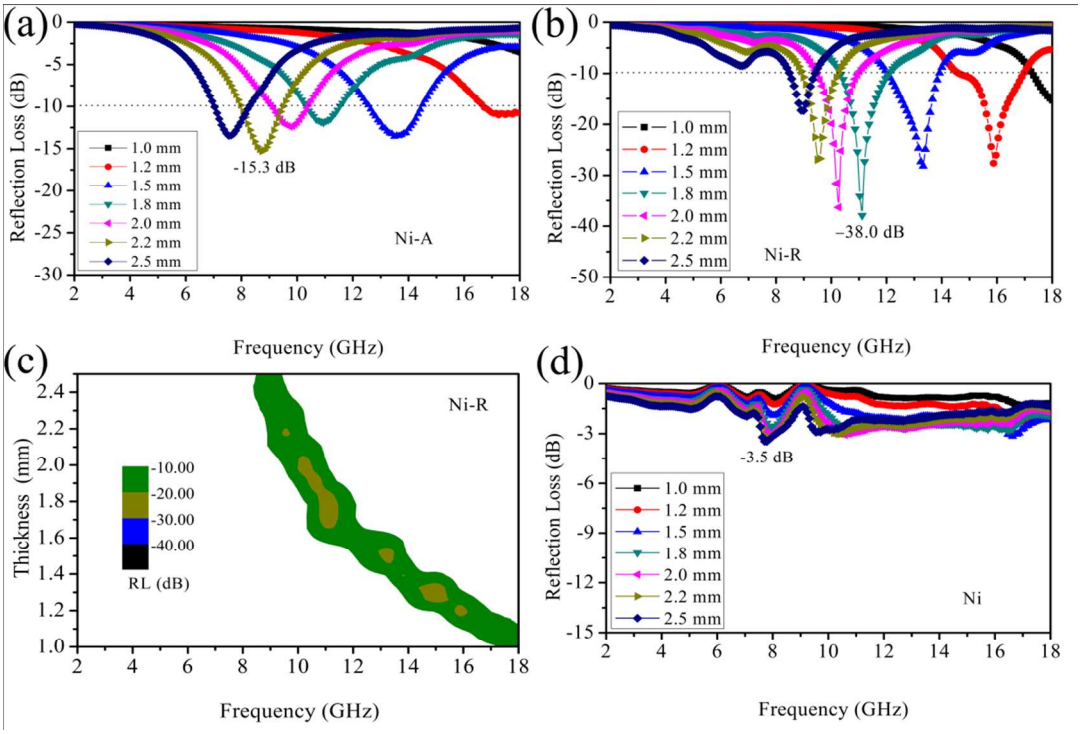

Fig. 11 Simulation of reflection loss (RL) of (a) Ni-A, (b) Ni-R and (d) Ni paraffin-composite with different thicknesses vs frequency; (c) contour map of the bandwidth with RL< −10 dB (90% microwave absorption) of Ni-R composite.

3.3. Microwave Absorption Performance

To reveal the microwave absorption properties of the as-synthesized samples, the reflection loss (RL) values of core-shell Ni-A and Ni-R composite microspheres were calculated using the relative complex permeability and permittivity at a given frequency and thickness layer according to the transmit line theory, which is summarized as the following equations: [9, 53]

$$RL = 20\log\left|(Z_{in} - Z_0)/(Z_{in} + Z_0)\right| \quad (5)$$

$$Z_{in} = Z_0\sqrt{\frac{\mu_r}{\varepsilon_r}}\tanh\left(j\frac{2\pi fd\sqrt{\mu_r\varepsilon_r}}{c}\right) \quad (6)$$

Where Z_0 is the impedance of free space, Z_{in} is the input characteristic impedance, f is the frequency, c is the velocity of light, and d is the thickness of the composites.

Fig. 11a shows the reflection loss versus frequency for Ni-A wax composite at the various thicknesses. The minimum reflection loss is –15.3 dB at 8.7 GHz with the thickness of 2.2 mm. In comparison with Ni-A composite, the Ni-R paraffin composite reveals better microwave absorption performance. As shown in **Fig. 11b**, the lowest reflection loss is –38.0 dB at 11.1 GHz and the corresponding thickness is 1.8 mm. The effective absorption (below -10 dB) bandwidth reaches 9.5 GHz (8.5 GHz-

Physical Chemistry Chemical Physics Accepted Manuscript

This journal is © The Royal Society of Chemistry [year]

18.0 GHz) for the absorber with the thin thickness in 1.0−2.5 mm. It can be found that the attenuation peaks would shift to lower frequencies with the increasing thickness. It can be explained by the quarter-wavelength cancellation model that the incident and reflected waves in the absorber are out of phase 180°, which gives rise to the reflected waves in the air-absorber interface totally canceled. [54, 55] **Fig. 11c** shows the bandwidth of the absorption frequency for RL< -10 dB in a two-dimensional contour plot. The result indicates that a thinner absorber layer has a wider frequency bandwidth. To probe the effect of TiO_2 on the microwave attenuation of Ni/TiO_2 composite, the reflection loss of bare Ni microspheres was also investigated (**Fig. 11d**). It is worth noting that the microwave absorption property of the pure Ni microspheres is very weak. In this work, core-shell structured Ni/TiO_2 composites exhibit outstanding microwave absorption compared with bare Ni particles (Fig.11), which can be explained as following: firstly, the impedance match can be improved after coating with TiO_2 shell and the eddy current effect can also be suppressed; secondly, the complementary effect between magnetic loss (Ni, low frequency) and dielectric loss (TiO_2, high frequency) is helpful for microwave absorption; thirdly, the interfacial polarization between Ni and TiO_2 is also favorable to microwave absorption.

The microwave absorption properties of individual TiO_2 are also investigated. As shown in **Fig. S1**, the microwave absorption properties of individual TiO_2 are very poor and the minimum reflection loss of TiO_2 particles is only –3.9 dB at 12.4 GHz. Moreover, the effect of the TiO_2 amounts on microwave absorption properties of Ni/TiO_2 heterostructure composites has been reported in our previous work. [56] In order to investigate the influences of core diameter on its microwave absorption properties, two mean diameters of Ni cores (500 nm, 250 nm) were also prepared. As shown in Fig.S2(b,e), after coating with TiO_2, the surfaces of 500 nm Ni (Fig.S2a) and 250 nm Ni cores (Fig. S2d) became coarser. Fig.S2(c,f) exhibits the microwave absorption properties of Ni/TiO_2 (500 nm Ni) and Ni/TiO_2 (250 nm) composites. Interestingly, it can be found that the microwave absorption properties of Ni/TiO_2 composites increase with decreasing diameters of Ni cores. From above analysis, it can be concluded that the electromagnetic absorption properties of Ni/TiO_2 composites were influenced by shell thickness and core diameter.

Based on the RL versus frequency patterns, it can be seen that the coating of the dielectric TiO_2 shell improves the electromagnetic wave absorption ability. According to transmission line theory, good absorbers are also determined by another important factor−high electromagnetic attenuation. The microwave attenuation was controlled by the attenuation constant α, which can be described as: [57, 58]

$$\alpha = \frac{\sqrt{2}\pi f}{c} \times \sqrt{(\mu''\varepsilon'' - \mu'\varepsilon') + \sqrt{(\mu''\varepsilon'' - \mu'\varepsilon')^2 + (\mu'\varepsilon'' + \mu''\varepsilon')^2}} \qquad (7)$$

where f is the frequency of the EM-wave and c is the velocity of light. **Fig. 12** shows the frequency dependence of the attenuation constant. The Ni-R endows biggest α in all frequency ranges, indicating the excellent attenuation or EM wave absorption.

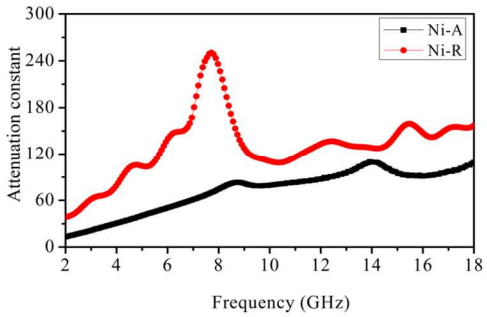

Fig.12 Attenuation constant of Ni/TiO_2 samples–paraffin composites versus frequency.

From above analysis, the Ni-R composite show the excellent microwave absorption in the measured frequency. The following several reasons should be noted: firstly, the Ni-R holds bigger EM attenuation α than Ni-A composite. Secondly, five relaxation processes occur in the Ni-R composites, which are higher than that of Ni-A. Thirdly, because of various sizes of rutile TiO_2 existing in the composite, more interfacial polarization processes occur between Ni-TiO_2, TiO_2-wax, and TiO_2-TiO_2, which are contributed to microwave absorption. Fourthly, the magnetic loss

Physical Chemistry Chemical Physics Accepted Manuscript

of Ni-R results from natural resonance, exchange resonance and eddy current loss. Finally, in the Ni/TiO_2 composite, thermal energy is generated due to the absorption of EM radiation, therefore, the materials should have sufficient thermal conductivity for heat dissipation. The thermal conductivity of material are largely determined by the preparation method, dimension of material, concentration of defects and the dispersant molecules adsorbed on the surface. [59] The thermal conductivity of anantase TiO_2 is reduced because of the presence of defects on anantase TiO_2 surface. Thus, the thermal conductivity of rutile TiO_2 is higher than that of anatase TiO_2,[60-62] which is beneficial for improving the microwave attenuation.

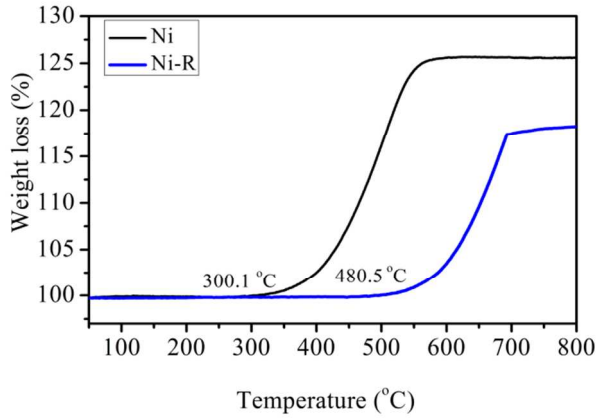

Fig. 13 TG spectra of the Ni and Ni-R composite microspheres.

As we known, anti-oxidant capacity is an important criterion for material application. The oxidation behaviors of the pure Ni and Ni-R are shown in **Fig. 13**. The bared Ni starts to oxidize at around 300 ºC. The pure Ni microspheres exhibit a obvious weight increase in the final stage due to the oxidation in air at high temperatures. After covering with a rutile TiO_2 shell, the oxidation temperature of Ni-R is increased to about 480 ºC. The complete oxidation is delayed to 750 ºC. It indicates that the core-shell Ni-R presents better oxidization resistance than that of Ni microsphere.

4. Conclusion

In summary, the core-shell Ni/TiO_2 microspheres with Ni cores and anantase or rutile TiO_2 shells were successfully prepared via solvothermal synthesis and annealing process. The effects of synthetic parameters on the crystal structure and morphology of Ni-A were investigated. The oxidation resistance of rutile TiO_2-coated Ni composite is better than that of the pure Ni microsphere. Compared with bared Ni, the microwave absorption properties can be significantly enhanced after coating with anantase or rutile TiO_2 shells. Among the two core-shell structured Ni/TiO_2 composite, rutile TiO_2 coated Ni (Ni-R) shows better microwave attenuation.. The minimum RL of Ni-R microspheres with the thickness of 1.8 mm reached –38.0 dB at 11.1 GHz. The absorption bandwidth with the reflection loss below -10 dB is 9.5 GHz by considering the thickness of 1.0−2.5 mm. The excellent absorption capabilities could be attributed to more relaxation and interfacial polarization processes, high thermal conductivity of rutile TiO_2. Our results demonstrate that the Ni-R core/shell microspheres prepared in current work are fascinating candidates for the new types of microwave absorbing materials with thin thickness and strong absorption.

Acknowledgements

This work was supported by the National Natural Science Foundation of China (Grant No. 51172213)

Notes and references

[a] *School of Materials Science and Engineering, Zhengzhou University, Zhengzhou 450001, China*

[b] *Laboratory of Aeronautical Composites, Zhengzhou Institute of Aeronautical Industry Management, Zhengzhou 450046, China*

** Corresponding Author.*

Dr. Gang Shao

E-mail address: gang_shao@zzu.edu.cn

Prof. Rui Zhang

Tel: +86-371-60632007

Fax: +86-371-60632600

E-mail address: zhangray@zzu.edu.cn

1. Y. Li, J. Zhang, Z. Liu, M. Liu, H. Lin and R. Che, *J. Mater. Chem. C*, 2014, **2**, 5216-5222.
2. X. Sun, J. He, G. Li, J. Tang, T. Wang, Y. Guo and H. Xue, *J. Mater. Chem. C*, 2013, **1**, 765-777.

Physical Chemistry Chemical Physics Accepted Manuscript

3. A. Wang, W. Wang, C. Long, W. Li, J. Guan, H. Gu and G. Xu, *J. Mater. Chem. C*, 2014, **2**, 3769-3776.
4. M. Yu, C. Liang, M. Liu, X. Liu, K. Yuan, H. Cao and R. Che, *J. Mater. Chem. C*, 2014, **2**, 7275-7283..
5. Q. Liu, B. Cao, C. Feng, W. Zhang, S. Zhu and D. Zhang*, Compos. Sci. Technol.,* 2012, **72**, 1632-1636.
6. M. Oyharçabal, T. Olinga, M.-P. Foulc, S. Lacomme, E. Gontier and V. Vigneras, *, Compos. Sci. Technol.,* 2013, **74**, 107-112.
7. A. Ohlan, K. Singh, A. Chandra and S. K. Dhawan, *ACS Appl. Mater. Interfaces*, 2010, **2**, 927-933.
8. Z. Liu, G. Bai, Y. Huang, F. Li, Y. Ma, T. Guo, X. He, X. Lin, H. Gao and Y. Chen, *J. Phys. Chem. C*, 2007, **111**, 13696-13700.
9. Z. Wang, L. Wu, J. Zhou, W. Cai, B. Shen and Z. Jiang, *J. Phys. Chem. C*, 2013, **117**, 5446-5452.
10. P.-B. Liu, Y. Huang and X. Sun, *ACS Appl. Mater. Interfaces*, 2013, **5**, 12355-12360.
11. H. Yu, T. Wang, B. Wen, M. Lu, Z. Xu, C. Zhu, Y. Chen, X. Xue, C. Sun and M. Cao, *J. Mater. Chem.*, 2012, **22**, 21679-21685.
12. Y. Ren, C. Zhu, S. Zhang, C. Li, Y. Chen, P. Gao, P. Yang and Q. Ouyang, *Nanoscale*, 2013, **5**, 12296-12303.
13. C. Cui, Y. Du, T. Li, X. Zheng, X. Wang, X. Han and P. Xu, *J. Phys. Chem. B*, 2012, **116**, 9523-9531.
14. P. Zhang, X. Han, L. Kang, R. Qiang, W. Liu and Y. Du, *RSC Adv.*, 2013, **3**, 12694-12701.
15. W. Li, T. Qiu, L. Wang, S. Ren, J. Zhang, L. He and X. Li, *ACS Appl. Mater. Interfaces*, 2013, **5**, 883-891.
16. W. Zhou, X. Hu, X. Bai, S. Zhou, C. Sun, J. Yan and P. Chen, *ACS Appl. Mater. Interfaces*, 2011, **3**, 3839-3845.
17. Y.-J. Chen, G. Xiao, T.-S. Wang, Q.-Y. Ouyang, L.-H. Qi, Y. Ma, P. Gao, C.-L. Zhu, M.-S. Cao and H.-B. Jin, *J. Phys. Chem. C*, 2011, **115**, 13603-13608.
18. X. G. Liu, D. Y. Geng, H. Meng, P. J. Shang and Z. D. Zhang, *Appl. Phys. Lett.*, 2008, **92**, 173117.
19. B. Zhao, G. Shao, B. Fan, W. Zhao, Y. Xie and R. Zhang, *RSC Adv.*, 2014, **4**, 61219-61225.
20. B. Zhao, G. Shao, B. Fan, W. Li, X. Pian and R. Zhang, *Mater. Lett.*, 2014, **121**, 118-121.
21. Y.-J. Chen, F. Zhang, G.-g. Zhao, X.-y. Fang, H.-B. Jin, P. Gao, C.-L. Zhu, M.-S. Cao and G. Xiao, *J. Phys. Chem. C*, 2010, **114**, 9239-9244.
22. S. Yan, L. Zhen, C. Xu, J. Jiang and W. Shao, *J. Phys. D: Appl. Phys.*, 2010, **43**, 245003.
23. Y.-J. Chen, P. Gao, R.-X. Wang, C.-L. Zhu, L.-J. Wang, M.-S. Cao and H.-B. Jin, *J. Phys. Chem. C*, 2009, **113**, 10061-10064.
24. X. L. Dong, X. F. Zhang, H. Huang and F. Zuo, *Appl. Phys. Lett.*, 2008, **92**, 013127.
25. Zhang, X.; Dong, X.; Huang, H.; Lv, B.; Lei, J.; Choi, C. *J. Phys. D: Appl. Phys.* **2007**, *40,* 5383..
26. L. Xi, Z. Wang, Y. Zuo and X. Shi, *Nanotechnology*, 2011, **22**, 045707.
27. G. Tong, Q. Hu, W. Wu, W. Li, H. Qian and Y. Liang, *J. Mater. Chem.*, 2012, **22**, 17494-17504.
28. C. Gong, J. Zhang, X. Zhang, L. Yu, P. Zhang, Z. Wu and Z. Zhang, *J. Phys. Chem. C*, 2010, **114**, 10101-10107.
29. C. Wang, X. Han, P. Xu, J. Wang, Y. Du, X. Wang, W. Qin and T. Zhang, *J. Phys. Chem. C*, 2010, **114**, 3196-3203.
30. X. Zhang, X. Dong, H. Huang, Y. Liu, W. Wang, X. Zhu, B. Lv, J. Lei and C. Lee, *Appl. Phys. Lett.*, 2006, **89**, 053115.
31. X. Liu, Z. Ou, D. Geng, Z. Han, Z. Xie and Z. Zhang, *J. Phys. D: Appl. Phys.*, 2009, **42**, 155004.
32. M. Dadfar and M. Dadfar, *J. Magn. Magn. Mater.*, 2012, **324**, 4204-4208.
33. A. Dey, S. De, A. De and S. De, *Nanotechnology*, 2004, **15**, 1277.

Physical Chemistry Chemical Physics Accepted Manuscript

34. H.-M. Xiao, X.-M. Liu and S.-Y. Fu, *Compos. Sci. Technol.*, 2006, **66**, 2003-2008.
35. J. Liu, R. Che, H. Chen, F. Zhang, F. Xia, Q. Wu and M. Wang, *Small*, 2012, **8**, 1214-1221.
36. C.-L. Zhu, M.-L. Zhang, Y.-J. Qiao, G. Xiao, F. Zhang and Y.-J. Chen, *J. Phys. Chem. C*, 2010, **114**, 16229-16235.
37. J. S. Chen, C. Chen, J. Liu, R. Xu, S. Z. Qiao and X. W. Lou, *Chem. Commun.*, 2011, **47**, 2631-2633.
38. J. Liu, J. Cheng, R. Che, J. Xu, M. Liu and Z. Liu, *J. Phys. Chem. C*, 2012, **117**, 489-495.
39. E. A. Barringer and H. K. Bowen, *Langmuir*, 1985, **1**, 414-420.
40. W. Li, J. Yang, Z. Wu, J. Wang, B. Li, S. Feng, Y. Deng, F. Zhang and D. Zhao, *J. Am. Chem. Soc.*, 2012, **134**, 11864-11867.
41. X.-L. Shi, M.-S. Cao, J. Yuan, Q.-L. Zhao, Y.-Q. Kang, X.-Y. Fang and Y.-J. Chen, *Appl. Phys. Lett.*, 2008, **93**, 183118.
42. L. Deng and M. Han, *Appl. Phys. Lett.*, 2007, **91**, 023119.
43. X. F. Zhang, P. F. Guan and X. L. Dong, *Appl. Phys. Lett.*, 2010, **97**, 033107.
44. X. a. Fan, J. Guan, W. Wang and G. Tong, *J. Phys. D: Appl. Phys.*, 2009, **42**, 075006.
45. S. He, G.-S. Wang, C. Lu, J. Liu, B. Wen, H. Liu, L. Guo and M.-S. Cao, *J. Mater. Chem. A*, 2013, **1**, 4685-4692.
46. D. Chen, H. Quan, G. S. Wang and L. Guo, *ChemPlusChem*, 2013, **78**, 843-851.
47. P. H. Fang, *J. Chem. Phys.*, 1965, **42**, 3411-3413.
48. X.-J. Zhang, G.-S. Wang, W.-Q. Cao, Y.-Z. Wei, M.-S. Cao and L. Guo, *RSC Adv.*, 2014, **4**, 19594-19601.
49. Y. Du, W. Liu, R. Qiang, Y. Wang, X. Han, J. Ma and P. Xu, *ACS Appl. Mater. Interfaces*, 2014, **6**, 12997-13006.
50. S. He, C. Lu, G.-S. Wang, J.-W. Wang, H.-Y. Guo and L. Guo, *ChemPlusChem*, 2014, **79**, 569-576.
51. J. Guo, X. Wang, P. Miao, X. Liao, W. Zhang and B. Shi, *J. Mater. Chem.*, 2012, **22**, 11933-11942.
52. T. Liu, P. Zhou, J. Xie and L. Deng, *J. Appl. Phys.*, 2012, **111**, 093905.
53. G. Sun, B. Dong, M. Cao, B. Wei and C. Hu, *Chem. Mater.,* 2011, **23**, 1587-1593.
54. R. Li, T. Wang, G. Tan, W. Zuo, J. Wei, L. Qiao and F. Li, *J. Alloys Compd.*, 2014, **586**, 239-243.
55. C. Wang, X. Han, X. Zhang, S. Hu, T. Zhang, J. Wang, Y. Du, X. Wang and P. Xu, *J. Phys. Chem. C*, 2010, **114**, 14826-14830.
56. B. Zhao, G. Shao, B. Fan, Y. Chen and R. Zhang, *Physica B*, 2014, **454**, 120-125.
57. J. Xiang, J. Li, X. Zhang, Q. Ye, J. Xu and X. Shen, *J. Mater. Chem. A*, 2014, **2**, 16905-16914.
58. S. L. Wen, Y. Liu, X. C. Zhao, J. W. Cheng and H. Li, *Phys. Chem. Chem. Phys.*, 2014, **16**, 18333-18340
59. M. M. Bernal, M. Martin-Gallego, I. Molenberg, I. Huynen, M. A. Lopez Manchado and R. Verdejo, *RSC Adv.*, 2014, **4**, 7911-7918.
60. S. M. Lee, D. G. Cahill and T. H. Allen, *Phys. Rev. B*, 1995, **52**, 253-257.
61. Y. Ding and B. Xiao, *Comput. Mater. Sci.*, 2014, **82**, 202-218.
62. J. Fang, C. Reitz, T. Brezesinski, E. J. Nemanick, C. B. Kang, S. H. Tolbert and L. Pilon, *J. Phys. Chem. C*, 2011, **115**, 14606-14614.

Physical Chemistry Chemical Physics Accepted Manuscript

This journal is © The Royal Society of Chemistry [year]